

Crystal structure of the M1 protein-binding domain of the influenza A virus nuclear export protein (NEP/NS2)

Hatice Akarsu^{1,2}, Wilhelm P. Burmeister^{1,2}, Carlo Petosa¹, Isabelle Petit¹, Christoph W. Müller¹, Rob W. H. Ruigrok^{1,2} and Florence Baudin^{1,2,3,4}

¹EMBL Grenoble Outstation, BP 181, 38042 Grenoble cedex 9, ²Laboratoire de Virologie Moléculaire et Structurale, EA 2939, Faculté de Médecine, Université Joseph Fourier, 38706 La Tronche and ³Institut de Biologie Structurale, UMR 5075 CEA-CNRS-UJF, 41 rue Jules Horowitz, 38027 Grenoble cedex 1, France

⁴Corresponding author
e-mail: baudin@embl-grenoble.fr

H. Akarsu, W. P. Burmeister and C. Petosa contributed equally to this work

During influenza virus infection, viral ribonucleo proteins (vRNPs) are replicated in the nucleus and must be exported to the cytoplasm before assembling into mature viral particles. Nuclear export is mediated by the cellular protein Crm1 and putatively by the viral protein NEP/NS2. Proteolytic cleavage of NEP defines an N-terminal domain which mediates RanGTP-dependent binding to Crm1 and a C-terminal domain which binds to the viral matrix protein M1. The 2.6 Å crystal structure of the C-terminal domain reveals an amphipathic helical hairpin which dimerizes as a four-helix bundle. The NEP–M1 interaction involves two critical epitopes: an exposed tryptophan (Trp78) surrounded by a cluster of glutamate residues on NEP, and the basic nuclear localization signal (NLS) of M1. Implications for vRNP export are discussed.

Keywords: Crm1 RanGTP/influenza A virus/M1 protein/NEP (NS2) protein/nuclear export

Introduction

Influenza virus has a single-stranded RNA genome composed of eight negative-sense RNA segments (reviewed by Lamb and Krug, 2001). The 3' and 5' ends of the viral RNA (vRNA) segments are bound to a heterotrimeric RNA-dependent RNA polymerase (Murti *et al.*, 1988), whereas the rest of the vRNA is encapsidated by the viral nucleoprotein (NP) (Klumpp *et al.*, 1997; Martín-Benito *et al.*, 2001). Inside the virus, the eight ribonucleoprotein particles (vRNPs) associate with the matrix protein M1, which in turn is bound to the viral membrane and the cytoplasmic tails of the glycoproteins. Following fusion of the viral and cellular membranes during infection, the vRNPs dissociate from M1 and are released into the cytoplasm (Martin and Helenius, 1991). They are then actively imported into the nucleus where viral transcription and replication take place (Whittaker *et al.*, 1996; Bui *et al.*, 2000). Newly synthesized vRNPs are subsequently exported to the

cytoplasm to form new virus particles at the plasma membrane.

The nuclear export of vRNPs is mediated by the cellular protein Crm1/exportin1 (Elton *et al.*, 2001; Ma *et al.*, 2001; Watanabe *et al.*, 2001), a member of the importin β family of nuclear transport receptors (reviewed in Weis, 2003). Crm1 mediates the nuclear export of numerous proteins bearing a leucine-rich nuclear export signal (NES) (Fornerod *et al.*, 1997; Fukuda *et al.*, 1997; Stade *et al.*, 1997). Like other exportins, the affinity of Crm1 for its NES-containing cargo is greatly enhanced in the presence of the small GTPase Ran. Indeed, formation of a cooperative ternary complex with Crm1 and RanGTP is good evidence that a given substrate is a bona fide export cargo of Crm1 (Fornerod *et al.*, 1997; Stade *et al.*, 1997). Crm1 also exports snurportin1, which lacks a leucine-rich NES (Paraskeva *et al.*, 1999), and certain viral RNA species. In particular, Crm1 mediates the export of unspliced HIV-1 mRNA via the adaptor protein Rev, which possesses a leucine-rich NES and binds to the Rev response element (RRE) of HIV-1 mRNA (Meyer and Malim, 1994; Fischer *et al.*, 1995; Askjaer *et al.*, 1998).

There is considerable evidence that the 14.5 kDa protein NEP ('nuclear export protein', formerly called NS2), behaves as an adaptor protein analogous to HIV-1 Rev by mediating the association of Crm1 with vRNPs. NEP associates with the matrix protein M1 (Yasuda *et al.*, 1993; Ward *et al.*, 1995), which binds vRNPs with high affinity (Baudin *et al.*, 2001) and whose nuclear localization is essential for vRNP export (Martin and Helenius, 1991; Whittaker *et al.*, 1996; Bui *et al.*, 2000). NEP contains a leucine-rich NES which can functionally replace that of Rev to mediate the nuclear export of RRE-containing RNAs, and which, when fused to a heterologous protein, directs the latter's export from mammalian cell nuclei (O'Neill *et al.*, 1998; Paragas *et al.*, 2001). Biochemical and yeast two-hybrid assays show that NEP interacts with Crm1 and with certain nucleoporins (Elton *et al.*, 2001; Paragas *et al.*, 2001). Anti-NEP antibodies block vRNP export when microinjected into the nucleus (O'Neill *et al.*, 1998), while recombinant virus lacking NEP is defective for vRNP export (Neumann *et al.*, 2000). Inhibition of Raf signalling results in impaired function of NEP and nuclear retention of vRNPs (Pleschka *et al.*, 2001).

Here we show that limited proteolysis of NEP defines an N- and C-terminal domain bearing Crm1- and M1-binding activities, respectively. We present the crystal structure of the C-terminal domain of NEP at 2.6 Å resolution and we identify the structural epitopes which mediate recognition of M1. Implications for vRNP export are discussed.

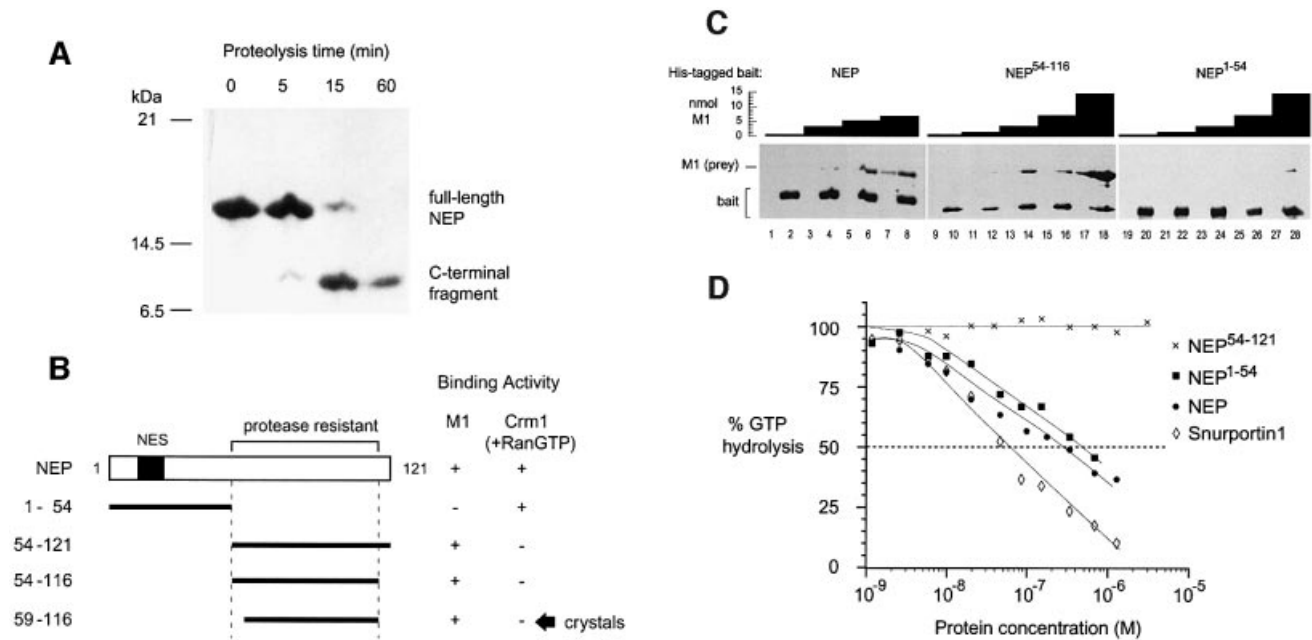


Fig. 1. Proteolysis of NEP defines two functionally distinct domains. **(A)** Proteolytic time course. NEP was incubated with elastase in a 1000:1 molar ratio at 20°C. The reaction was stopped with 1 mM phenylmethylsulfonyl fluoride (PMSF) at the times shown. **(B)** Summary of deletion mutants. Fragment NEP⁵⁹⁻¹¹⁶ was obtained by subtilisin cleavage of NEP⁵⁴⁻¹¹⁶. **(C)** The C-terminal domain of NEP mediates binding to M1. Nickel-agarose beads preincubated with a His-tagged NEP construct ('bait') (even-numbered lanes) or buffer (odd-numbered lanes) were incubated with the indicated amounts of untagged M1 ('prey'). After washing, bound proteins were eluted and analyzed by denaturing gel electrophoresis. **(D)** The N-terminal domain of NEP mediates RanGTP-dependent binding to Crm1. Ran- $[\gamma\text{-}^{32}\text{P}]\text{GTP}$ and Crm1 were incubated with various concentrations of snurportin1 or an NEP construct. The GTPase reaction was initiated by addition of RanGAP and hydrolysis of Ran-bound GTP was determined as ^{32}P release. Both NEP and NEP¹⁻⁵⁴, but not NEP⁵⁴⁻¹²¹, bound cooperatively with RanGTP to Crm1, causing a decrease in GTP hydrolysis. Data points represent the mean of three independent measurements, and in all cases the standard deviation did not exceed 10% of the mean value.

Results and discussion

Proteolysis of NEP defines an N-terminal domain with RanGTP-dependent Crm1 binding activity and a C-terminal M1-binding domain

Because we were unable to obtain crystals of full-length NEP we used limited proteolysis to probe the domain structure of NEP. Recombinant NEP purified from *Escherichia coli* and treated with elastase, trypsin or chymotrypsin yielded a proteolytically resistant fragment of ~7 kDa (Figure 1A), identified by N-terminal sequencing and mass spectrometry to comprise residues 54–116. In contrast, the N-terminal half bearing the NES motif appeared to be rapidly degraded. Similar results have been reported for the digestion of NEP with either trypsin or V8 protease (Lommer and Luo, 2002). Based on these findings, we constructed deletion mutants NEP¹⁻⁵⁴ and NEP⁵⁴⁻¹²¹ (Figure 1B). Both constructions yielded soluble proteins when expressed in *E.coli*.

To test these constructs for M1 binding activity, we performed pull-down assays in which nickel-agarose beads preincubated with a His-tagged NEP construct were subsequently incubated with untagged M1 (Figure 1C). Although some M1 bound non-specifically to beads in the absence of NEP (lane 7), binding was substantially enhanced in the presence of NEP (lanes 4, 6 and 8), reflecting a direct association between NEP and M1. M1 exhibited a roughly similar degree of binding toward NEP⁵⁴⁻¹²¹ as toward NEP (lanes 9–18), but had comparatively little affinity for NEP¹⁻⁵⁴ (lanes 19–28). Thus,

NEP⁵⁴⁻¹²¹ appears to mediate the interaction with M1. This agrees with a previous report implicating the C-terminal 70 residues of NEP in binding M1 (Ward *et al.*, 1995).

To test the NEP deletion mutants for their ability to function as a nuclear export cargo for Crm1, we performed a kinetic assay routinely used to measure RanGTP-dependent Crm1 binding activity (Bischoff *et al.*, 1995). This assay exploits the fact that GTP hydrolysis by Ran is stimulated by the RanGTPase activating protein (RanGAP) but inhibited by the association of RanGTP with Crm1. In a reaction mixture containing Crm1, RanGTP and RanGAP, the addition of a nuclear export cargo enhances the affinity of Crm1 for RanGTP, thereby causing a reduced rate of GTP hydrolysis, whereas substrates which fail to bind Crm1 or bind independently of RanGTP have no effect. As a positive control we tested snurportin1, a trimethylguanosine ($m^3\text{G}$) cap binding protein which is efficiently exported by Crm1 (Paraskeva *et al.*, 1999). We observed a 50% reduction in GTP hydrolysis in the presence of 50 nM snurportin1 (Figure 1D), in agreement with published results (Paraskeva *et al.*, 1999). Next, we confirmed that full-length NEP behaved as a Crm1 export cargo in this assay: as little as 8 nM NEP yielded a detectable decrease in GTP hydrolysis, while 500 nM NEP gave a 50% reduction (Figure 1D). Thus the apparent affinity of Crm1 for NEP is similar to that reported for HIV Rev (Paraskeva *et al.*, 1999). Finally, we tested the two NEP deletion mutants. Consistent with the presence of the Leu-rich NES motif, the NEP¹⁻⁵⁴ construct showed significant RanGTP-dependent Crm1 binding activity which was comparable

Table I. Data collection, phasing and refinement statistics

	Native	PtCl ₄ derivative (I)	PtCl ₄ derivative (II)	OsCl ₆ derivative
Data collection				
Resolution (Å)	2.6 (2.74–2.60)	3.50 (3.69–3.50)	3.50 (3.69–3.50)	2.8 (2.95–2.80)
Completeness	0.996 (1.000)	0.991 (0.986)	1.000 (1.000)	0.965 (0.817)
Multiplicity	3.8 (3.8)	6.7 (6.8)	14.9 (15.5)	6.0 (3.1)
<i>I</i> / σ	6.0 (2.0)	5.5 (2.3)	3.4 (2.0)	4.9 (3.9)
<i>R</i> _{merge}	0.090 (0.32)	0.083 (0.326)	0.102 (0.330)	0.093 (0.168)
<i>R</i> _{anomalous}		0.065 (0.148)	0.063 (0.107)	0.043 (0.147)
Phasing				
Overall FOM	Overall 0.33	At 4.6 Å: 0.71	At 3.4 Å: 0.28	At 2.9 Å: 0.06
FOM after RESOLVE	Overall 0.54	At 4.6 Å: 0.89	At 3.3 Å: 0.60	At 2.6 Å: 0.15
Refinement				
No. of reflections working set	6962			
<i>R</i> _{cryst}	0.176 (0.225)			
<i>R</i> _{free}	0.244 (0.319)			
Average <i>B</i> factor (Å ²)	43.5			
R.m.s. bonds (Å)	0.043			
R.m.s. angles (°)	3.3			

A test set containing 5% of the reflections was used throughout the refinement. Values for the highest resolution bin are given in parentheses.

to that of the full-length protein (Figure 1D). In contrast, the addition of NEP^{54–121} had no effect on GTP hydrolysis, even at the highest concentration tested (20 μ M) (Figure 1D). Thus NEP appears to be a modular protein composed of a protease-sensitive N-terminal domain which mediates RanGTP-dependent Crm1 binding, and a protease-resistant C-terminal domain chiefly responsible for M1 binding.

Crystal structure of the NEP C-terminal domain

Although NEP^{1–54} failed to crystallize and NEP^{54–121} yielded crystals of only poor quality, we could obtain well-diffracting crystals by digesting a slightly shorter construct (NEP^{54–116}) with subtilisin to obtain the C-terminal fragment NEP^{59–116} (Figure 1B). Crystals belong to space group *P*3₂21, with cell parameters *a* = *b* = 82.7 Å, *c* = 61.1 Å, and two molecules per asymmetric unit. Phases obtained using two heavy-atom derivatives resulted in a 2.6 Å experimental map which was readily interpreted (Table I). The final model, with *R*_{cryst} = 0.176 and *R*_{free} = 0.244, includes residues 63–116 and 48 water molecules. Residues 59–62 are disordered.

The C-terminal NEP domain forms a helical hairpin with approximate dimensions 40 × 25 × 15 Å (Figure 2A). Residues 64–85 and 94–115 comprise helices C1 and C2, respectively, while residues 86–93 form the interhelical turn. The two helices are equal in length and nearly perfectly antiparallel, giving the structure a remarkably flat appearance. Because of their shallow crossing angle (14°), the two helices share extensive contacts over their entire length, the majority of which are hydrophobic in nature. These are mediated by a total of 12 hydrophobic and four polar residues, with the two helices contributing one or two side chains from each of their six helical turns (Figure 2A and B). The hairpin is further stabilized by interactions involving three arginine residues from helix C1: Arg84 forms a hydrogen bond with glutamine Gln96, Arg77 forms a bifurcated salt bridge with glutamates Glu74 and Glu110, and Arg66 has its guanidium group favourably located near backbone

carbonyl groups at the C-terminus of helix C2, such that its positive charge interacts with the helix dipole (Figure 2A). The eight residues forming the interhelical turn are well ordered (average *B* factors resemble those of helical residues) and include two hydrophobic residues partially buried between the helices. Thus the C-terminal domain is a highly compact unit with little flexibility, explaining its resistance to proteolytic digestion.

The helical hairpin is strikingly amphipathic, with one face hydrophobic and the other hydrophilic (Figure 2C and D). The former contains 16 of the 21 hydrophobic residues present in the domain; these form a broad swathe that extends from the top to the bottom of the hairpin (Figure 2D, bottom left). In contrast, the opposite face bears 15 of the domain's 19 charged residues, almost all of which are located on helix C1. Six glutamate side chains cluster near the centre of this face, whereas basic residues localize to the top and bottom (Figure 2D, top right). This face also contains five hydrophobic residues (Figure 2D, bottom right). Four of these (Ile97, Met100, Leu103 and Leu107) form a continuous groove on the surface; the fifth is a prominently exposed tryptophan (Trp78) located in the centre of the glutamate cluster.

The isolated NEP C-terminal domain is a dimer

In the crystal structure, the hydrophobic face of one helical hairpin is buried against that of a second hairpin, related to the first by a non-crystallographic dyad. The two form an antiparallel four-helix bundle, with helix C1 from one hairpin packing against helix C2 of the other, and all four N- and C- termini located at one end (Figure 3A). The interface between the two monomers buries an accessible surface area of 1268 Å², representing 27% of the total surface area. Comparable values have been observed for homodimers of a similar molecular weight (Jones and Thornton, 1996) and for protein–protein interfaces in general (Lo Conte *et al.*, 1999). Twenty-four residues from each hairpin interact with residues from the other monomer (Figure 2B). Most of these residues mediate hydrophobic contacts, and with only a few exceptions are

identical to those mediating intramonomer contacts between the C1 and C2 helices. These residues are located near the 2-fold axis in each of the six layers defined by the turns of the four helices (Figure 3A). Interactions within and between layers give the helical bundle a tightly packed hydrophobic core, similar to that observed in the interior of globular proteins. Additional interactions stabilizing the dimer are a hydrogen bond between Glu95 and the backbone carbonyl group of Val83, and a salt bridge between Lys72 and glutamates Glu108 and Glu112 (Figure 3A).

The many interactions between the two monomers and the hydrophobic nature of the interface suggest that the observed dimer is not merely an artefact of crystallization, but represents the state of the NEP C-terminal fragment in solution. Indeed, unlike the monomer, the dimer has relatively few solvent-exposed hydrophobic residues and thus is more consistent with the highly soluble nature of this fragment. To verify this, we performed analytical gel filtration on NEP⁵⁴⁻¹¹⁶ and on full-length NEP, which is known to be monomeric (Lommer and Luo, 2002). Despite their nearly 2-fold difference in molecular weight (8.5 versus 14.5 kDa), both NEP⁵⁴⁻¹¹⁶ and full-length NEP elute at the same volume, corresponding to that expected for a globular protein of 15 kDa (Figure 3B). Given that the crystal structures of monomeric and dimeric NEP⁵⁹⁻¹¹⁶ are both highly compact (i.e. essentially globular), the result is consistent with the C-terminal fragment being dimeric in solution. This conclusion is further supported by the results of a cross-linking study. NEP treated with the cross-linking reagent ethylene glycol bis-succinimidylsuccinate (EGS) yields essentially a single band on a denaturing gel, consistent with a monomeric species (Figure 3C, lanes 1–4). In contrast, treatment of NEP⁵⁹⁻¹¹⁶ results in the appearance of a second band whose size corresponds to that expected for a dimer (lanes 5–8).

In these experiments, identical results were obtained regardless of whether the C-terminal fragment was expressed from a plasmid or obtained by proteolysis of the full-length protein. Therefore we conclude that proteolytic degradation of the N-terminal domain leads to spontaneous dimerization of the C-terminal domain. A likely explanation is that the N-terminal domain packs against the hydrophobic face of the C-terminal domain in the structure of full-length NEP, sterically hindering access to the dimerization interface; thus proteolysis would remove this steric hindrance. Burial of the hairpin's hydrophobic face by the N-terminal domain would also explain why full-length NEP is highly soluble in the absence of detergents.

NEP/M1 binding is mediated by the NLS motif of M1 and residue Trp78 of NEP

In order to localize the sites of interaction between NEP and M1, we set out to find mutants deficient for binding activity. M1 is known to consist of two domains: an N-terminal domain (residues 1–164), for which the crystal structure is known (Sha and Luo, 1997; Arzt *et al.*, 2001), and a C-terminal domain (residues 165–252) that mediates vRNP binding (Baudin *et al.*, 2001). Pull-down assays performed as above show that NEP⁵⁴⁻¹¹⁶ associates with the N-terminal, but not the C-terminal, domain of M1 (Figure 4B; data not shown). Because NEP has previously

been reported to bind an M1 fragment lacking residues 1–88 (Yasuda *et al.*, 1993), we conclude that a critical NEP binding epitope is located within the M1 N-terminal domain between residues 89 and 164. In the crystal structure of M1¹⁻¹⁶⁴, residues 89–164 form a four-helix bundle constituting a compact subdomain. This subdomain includes an exposed basic motif ¹⁰¹RKLLKR¹⁰⁵ that mediates binding to negatively charged liposomes (Baudin *et al.*, 2001) and is recognized by the cellular import machinery as a nuclear localization signal (NLS) (Ye *et al.*, 1995; Liu and Ye, 2002). We tested the ability of NEP to bind to M1^{mutNLS}, an M1 mutant in which the four basic residues of the NLS are replaced by alanines (¹⁰¹AALAA¹⁰⁵). This mutant was found to have severely reduced NEP binding affinity (Figure 4C). Failure to bind NEP cannot be ascribed to misfolding of the mutant protein, as its N-terminal domain (residues 1–164) has essentially the same crystal structure as that of wild-type M1 (unpublished results). It has been reported that M1 protein bearing a single mutation of either Lys102 or Lys104 is no longer imported into the nucleus of infected cells and results in lethality 72 h after transfection, whereas mutation of R101 or R105 has little effect on M1 nuclear import or RNP export (Liu and Ye, 2002). To assess the relative contribution of the two half-sites of the NLS motif to NEP binding, we constructed double point mutants of M1 in which either residues Arg101 and Lys102 or residues Lys104 and Arg105 were simultaneously replaced by alanine residues (mutants M1^{R101A, K102A} and M1^{K104A, R105A}, respectively). In pull-down experiments, both mutants bound NEP more weakly than wild-type M1 but more strongly than the M1^{mutNLS} mutant which lacks all four basic residues (compare Figure 4A and C with D and E). This indicates that at least one basic residue from each NLS half-site contributes to NEP binding, and that residues in both half-sites are required for full binding activity. Masking of the NLS motif by NEP may ensure that newly exported progeny vRNPs destined for virus assembly at the plasma membrane are not reimported into the nucleus.

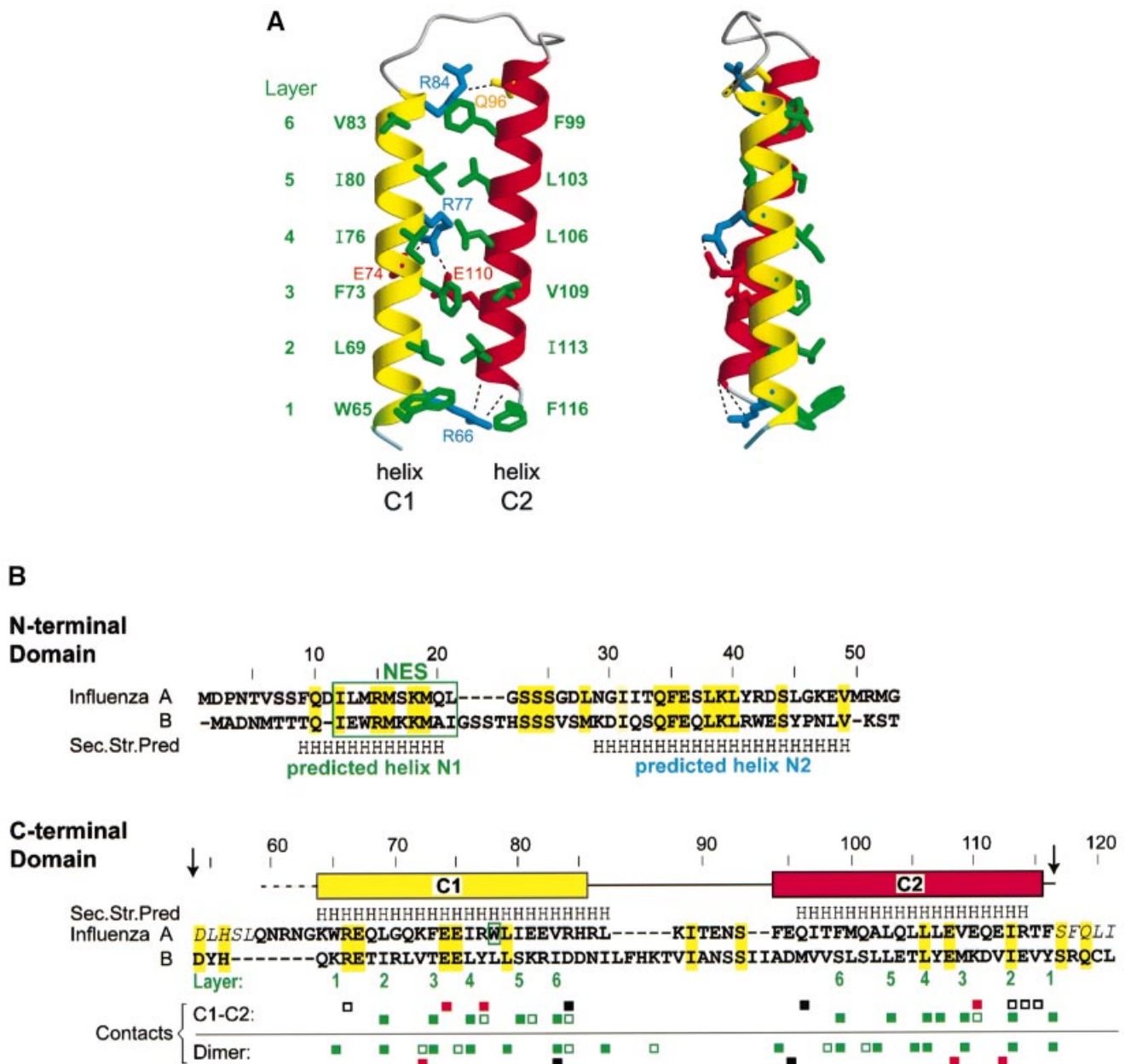
We next set out to localize the M1 binding site on NEP. We focused on residues which are solvent exposed in the structure of the NEP⁵⁹⁻¹¹⁶ dimer, reasoning that residues buried in the dimer were probably also buried in full-length NEP (and hence unable to mediate binding). Thus we examined the hydrophilic face of the helical hairpin, which is not involved in dimer formation, for possible binding epitopes. As described above, a conspicuous feature of this face is the prominently exposed Trp78 residue surrounded by a ring of glutamate residues (Figure 2D). This tryptophan is probably similarly exposed in full-length NEP, as near-UV circular dichroism (CD) and fluorescence spectroscopy have shown that the three aromatic residues in NEP are highly solvent accessible and able to rotate freely (Lommer and Luo, 2002). Therefore we constructed an NEP mutant in which Trp78 was replaced by a serine (NEP^{W78S}). We also made a double mutant in which residues Glu81 and Glu82 were substituted by alanines (NEP^{E81A, E82A}). These glutamates have their side chains located next to Trp78 but are not conserved in influenza B virus, where they are replaced by basic residues (Figure 2B and D). A pull-down assay shows that, whereas the double mutant retains significant affinity

for M1, mutation of Trp78 severely disrupts binding activity (Figure 4F and G). Both mutant proteins appear to fold correctly, as they behave similarly to the wild-type species in gel filtration chromatography and CD spectroscopy (data not shown). We conclude that Trp78 is a major M1 binding epitope of NEP.

Given the large number of glutamate residues near Trp78, the interaction between NEP and the basic NLS of M1 probably has a significant electrostatic component. Tryptophan residues play an important role in NLS recognition by the nuclear import factor importin α , where they buttress lysine side chains of the NLS so that these can interact favourably with acidic residues of importin α (Conti *et al.*, 1998; Conti and Kuriyan, 2000). Whether NEP recognizes the NLS motif of M1 by similar interactions must await determination of the structure of the M1/NEP complex.

Comparison of NEP proteins from type A and B influenza viruses

Although the NEP sequences from influenza A and B viruses share only 27% sequence identity (26% over the C-terminal domain), the chemical nature of residues is conserved at most positions, suggesting a common tertiary structure (Figure 2B). In particular, in the C-terminal domain the amphipathic nature of the helical hairpin and the highly charged character of helix C1 are preserved. Compared with influenza A, seven additional residues are present within the C-terminal domain of influenza B NEP, inserted between the C1 and C2 helices. These residues can be readily accommodated within the helical hairpin structure by a more elaborate interhelical loop or by extending one or both helices. Interestingly, the Trp78 residue implicated in M1 binding is replaced by a leucine in influenza B, suggesting that M1 recognition by NEP is



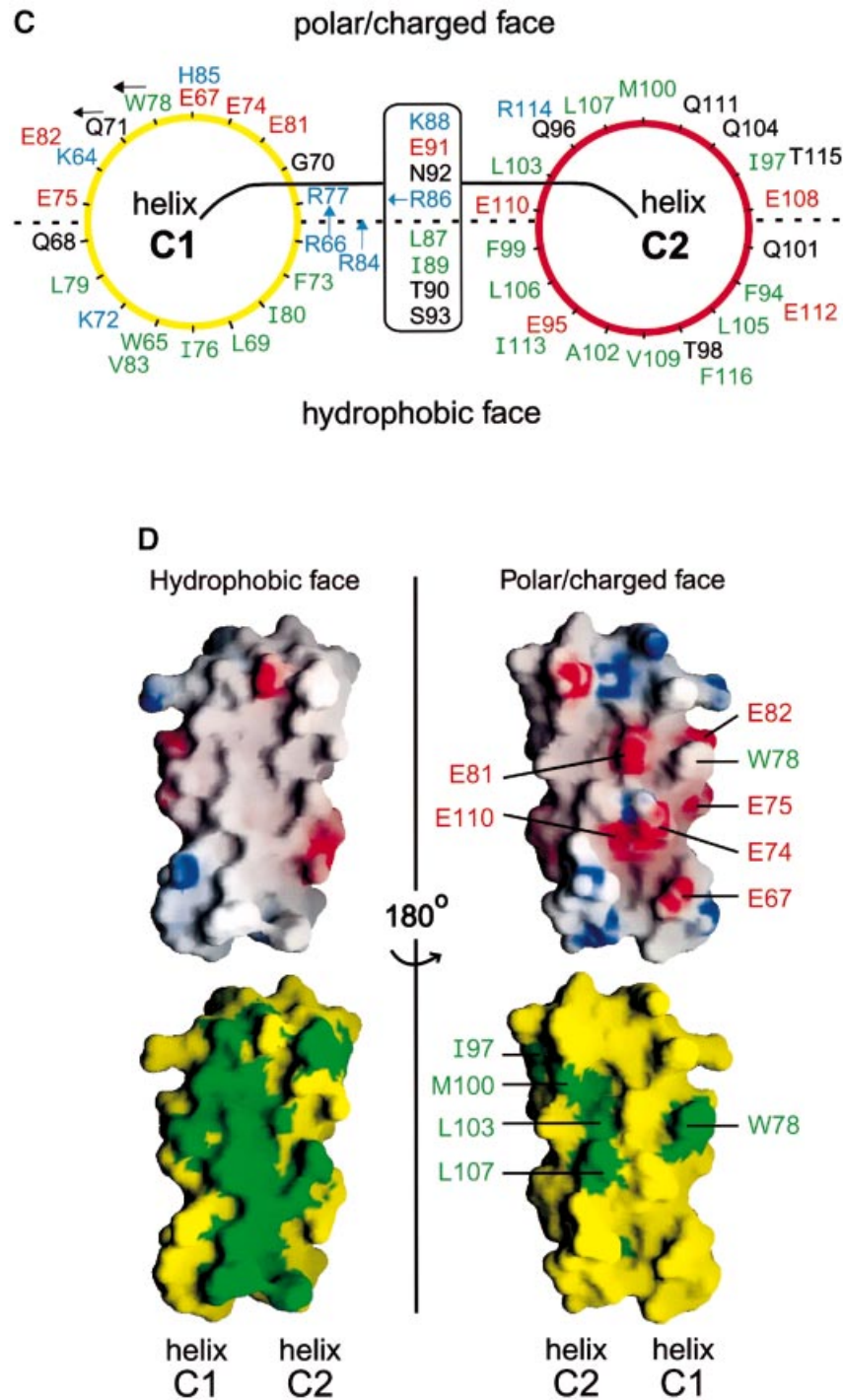


Fig. 2. Structure of the NEP C-terminal domain. (A) Ribbon diagram. The six layers of hydrophobic residues involved in interhelical contacts are shown. Also shown are the hydrogen bond between Arg84 and Gln96, the capping interaction between Arg66 and the C-terminus of helix C2, and the salt bridge involving Arg77, Glu74 and Glu110. For clarity, not all interhelical contacts are shown. (B) Sequence and secondary structure of NEP. Residues conserved between influenza A and B viruses are highlighted in yellow and grey. Residues predicted by the program PHD to be helical with >90% probability are labelled H. The NES motif and residue Trp78 implicated in M1 binding are boxed. Arrows mark limits of the proteolytically resistant fragment; residues in italics are absent from the construct used for structure determination; disordered residues are indicated by the dotted line. Contacts between helices C1 and C2 within one monomer, and those between two monomers of the dimer are indicated as follows: green squares, van der Waals contact involving a hydrophobic residue (filled square) or the aliphatic moiety of a polar residue (empty square); red square, salt bridge; filled black square, hydrogen bond; empty black square, capping interaction of Arg66 with C-terminus of helix C2. Typically, residues from helix C1 interact with those from helix C2 of the same or an adjacent layer. (C) Schematic diagram showing side-chain distribution. Helix C1 is viewed from C- to N-terminus and helix C2 from N- to C-terminus. Hydrophobic, polar, acidic and basic residues are coloured green, black, red and blue, respectively. The side chains of Arg66 and Arg84 emerge from the polar/charged face; those of Gln71, Trp78 and Arg86 point as shown by the arrows. (D) Surface properties of the C-terminal domain. Upper panels: electrostatic surface potential plotted from -10 kT (red) to +10 kT (blue). Lower panels: distribution of hydrophobic (green) and hydrophilic (yellow) side chains. The upper and lower left panels are in the same orientation as (A). The figure was produced using GRASP (Nicholls *et al.*, 1991).

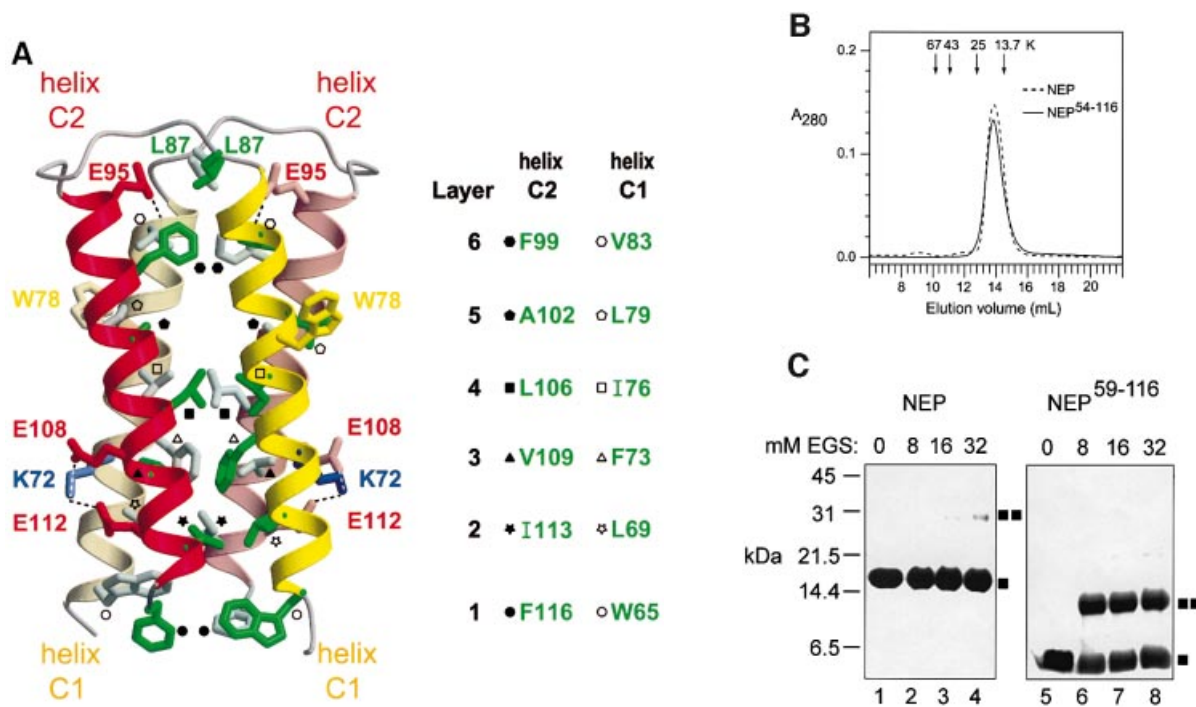


Fig. 3. The NEP C-terminal domain dimer. (A) Ribbon diagram of the four-helix bundle. The two monomers belong to the same asymmetric unit, related by a non-crystallographic dyad running nearly parallel to the individual helices. Six successive layers of interacting side chains define the hydrophobic core. Each of the helices in the bundle contributes one or more side chains per layer, with symmetry-related residues in the same layer. Not all residues in the dimerization interface are shown (but see Figure 2B). Hydrophobic residues in the dimer interface are identified in the legend to the right. Also shown are residue Trp78 implicated in M1 binding, the hydrogen bond between Glu95 and the backbone carbonyl of Val83, and the salt bridge involving Lys72, Glu108 and Glu112. (B) Analytical gel filtration of NEP and NEP⁵⁴⁻¹¹⁶. Arrows (from left to right) indicate elution volumes of the globular reference proteins bovine serum albumin, ovalbumin, chymotrypsinogen A and RNase A. The elution volumes of NEP (14.5 kDa) and NEP⁵⁴⁻¹¹⁶ (8.5 kDa) are nearly identical, suggesting that the latter is a dimer in solution. (C) Cross-linking experiment. NEP or NEP⁵⁹⁻¹¹⁶ was incubated with the indicated amount of EGS for 1 h on ice. Reactions were quenched by adding 100 mM Tris and analyzed by denaturing gel electrophoresis. Squares indicate the positions of monomers and dimers. Small amounts of the dimeric NEP and tetrameric NEP⁵⁹⁻¹¹⁶ species at high EGS concentrations are probably due to transient interactions between molecules in solution.

somewhat different between the two viral types. Indeed, the M1 NLS motif in influenza A, (¹⁰¹RKLKR¹⁰⁵) differs from the corresponding motif in influenza B (RKMRR) at two positions. We speculate that the replacement of NEP residue Trp78 by the shorter Leu side chain is compensated by the replacement of M1 residues Leu103 and Lys104 by the longer Met and Arg side chains, permitting the mode of M1–NEP interaction to be essentially preserved between the two viral types.

Speculations about vRNP export

Although NEP putatively mediates the association of Crm1 with vRNPs, we have been unable to detect a direct interaction *in vitro* between NEP and either NP or RNP (data not shown). This suggests that M1 may mediate the association of NEP with vRNPs, consistent with the interaction of M1 with vRNPs being essential for export (Martin and Helenius, 1991; Whittaker *et al.*, 1995; Bui *et al.*, 2000). Epitopes located in different domains of NEP mediate binding to M1 and Crm1, just as epitopes in different domains of M1 mediate binding to NEP and vRNP. Therefore it is possible that a ‘daisy-chain’ complex of Crm1, NEP, M1 and vRNP exists without the individual binary interactions interfering with one another (Figure 5A). Indirect evidence for this comes from

a GTPase assay in which Crm1 and RanGTP are incubated with NEP (Figure 5B). Neither the addition of M1 nor that of M1 plus vRNPs significantly alters the ability of NEP to inhibit GTP hydrolysis. Thus RanGTP-dependent recognition of NEP by Crm1 appears to be compatible with the presence of M1 and vRNP. The use of two adaptor proteins (NEP and M1) instead of just one between Crm1 and vRNP may offer influenza virus the possibility of greater regulatory control, especially since NEP binds the NLS motif of M1, an epitope involved in many other interactions. Masking of the NLS motif of M1 by NEP could ensure that the complex is not directly reimported to the nucleus when exported towards the cytoplasm. The putative use of two adaptor proteins for vRNP export is reminiscent of the situation in Crm1-mediated U snRNA export: Crm1 binds to the adaptor protein PHAX, which in turn recognizes a second adaptor, CBC, bound directly to U snRNA (Ohno *et al.*, 2000).

We note that, of the viral components tested, only NEP binds Crm1 cooperatively with RanGTP (Figure 5B). NP has also been proposed to mediate vRNP export, as it encapsidates vRNA, shuttles between the nucleus and the cytoplasm (Whittaker *et al.*, 1996; Neumann *et al.*, 1997) and interacts directly with Crm1 *in vitro* (Elton *et al.*, 2001). We have confirmed that Crm1 interacts directly

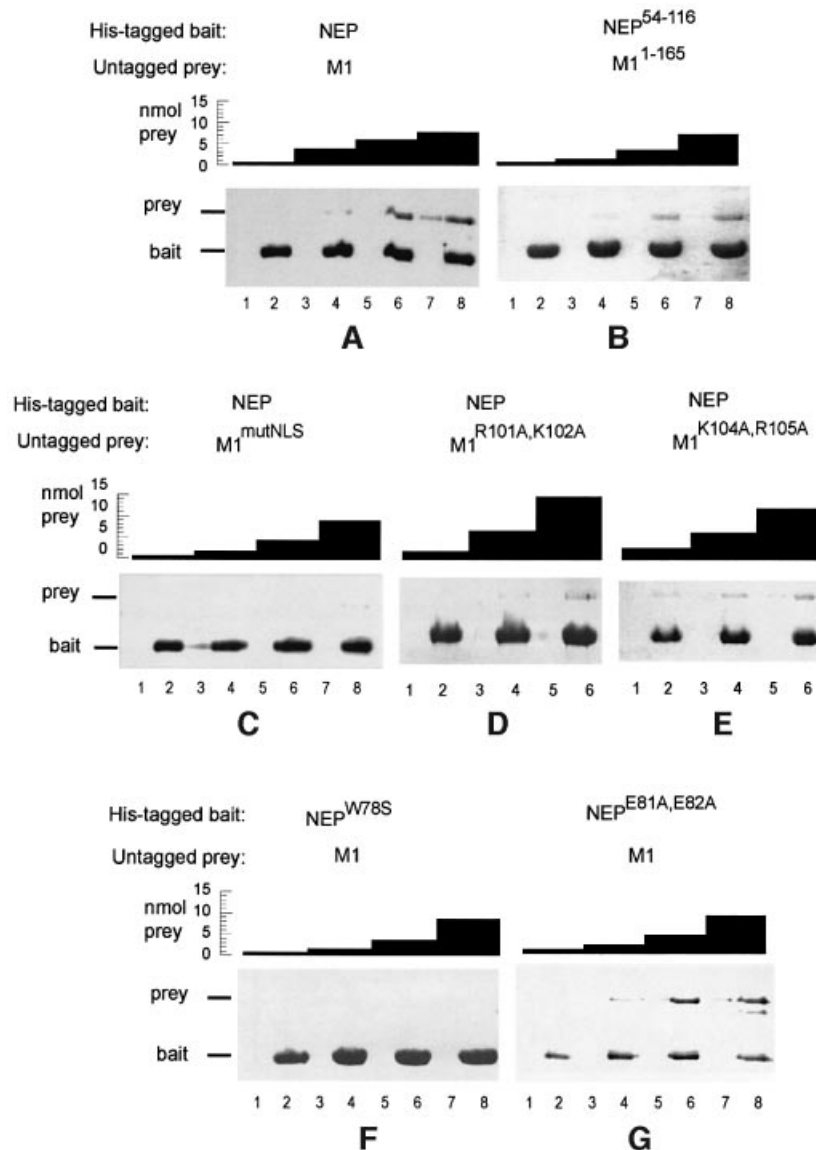


Fig. 4. NEP residue Trp78 and the NLS of M1 mediate NEP–M1 binding. Nickel–agarose beads preincubated with a His-tagged NEP construct ('bait') (even-numbered lanes) or buffer (odd-numbered lanes) were incubated with the indicated amounts of untagged M1 or an M1 mutant ('prey'). After washing, bound proteins were eluted and analyzed by denaturing gel electrophoresis. (A) NEP binds to M1. (B) The C-terminal NEP domain binds to the N-terminal domain of M1. (C) Mutation of the NLS motif in M1 severely reduces binding to NEP. (D) Mutation of R101 and K102 residues in M1 reduces binding to NEP. (E) Mutation of K104 and R105 residues in M1 reduces binding to NEP. (F) Mutation of NEP residue Trp78 disrupts binding to M1. (G) Mutation of NEP residues Glu81 and Glu82 has little effect on binding to M1.

with vRNP in a cosedimentation assay (not shown); however, our GTPase assay suggests that this interaction is not RanGTP dependent (Figure 5B).

The efficient passage of particularly large molecules through the nuclear pore complex has been shown to require the recruitment of more than one nuclear transport receptor (Ribbeck and Görlich, 2002). Indirect evidence suggesting that several Crm1 molecules are required for Rev-mediated export of unspliced HIV mRNA is the observation that export critically depends on the cooperative assembly of Rev multimers on the Rev response element (RRE). For example, stem-loop IIB within the RRE has high affinity for Rev monomers but is unable to direct Rev-mediated RNA export (Huang *et al.*, 1991; Mann *et al.*, 1994), while Rev variants or

mutants unable to form multimeric complexes are defective in the nuclear export of unspliced RRE-containing mRNAs (Malim *et al.*, 1989; Malim and Cullen, 1991; Thomas *et al.*, 1998). Similar evidence is lacking for the export of influenza vRNPs, but their large size (average ~5 MDa) suggests that they may also recruit several Crm1 molecules. Although the precise M1:vRNP binding stoichiometry during export is undetermined, the results from a number of studies suggest that an individual vRNP can bind several M1 molecules (Watanabe *et al.*, 1996; Ye *et al.*, 1999; Baudin *et al.*, 2001). Thus association of NEP with more than one of these would permit a single vRNP to recruit multiple Crm1 molecules (Figure 5A). Experiments to test this hypothesis are currently under way.

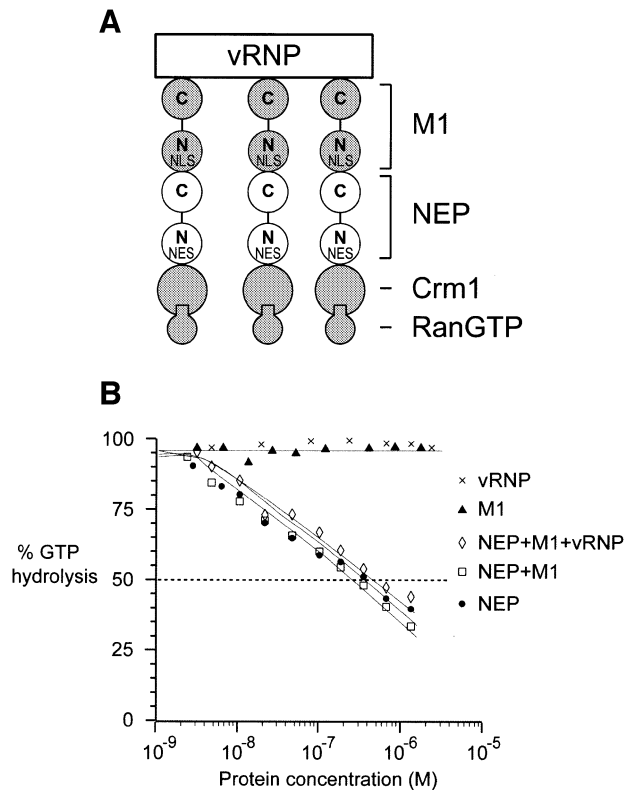


Fig. 5. Possible interactions among influenza viral components. (A) A hypothetical export complex. Crm1/RanGTP binds to NEP, NEP binds to M1 and M1 binds to vRNP. The binding surfaces involved in the individual interactions are spatially distinct. The N- and C-terminal domains and NLS and NES motifs of M1 and NEP are indicated. A single vRNP may recruit several molecules of Crm1. (B) RanGTPase assay involving several viral components. The assay was performed essentially as for Figure 1D. NEP, but not M1 or vRNP, binds to Crm1 cooperatively with RanGTP. NEP preincubated with an equimolar amount of M1 or with M1 plus vRNP behaves similarly to NEP alone.

Materials and methods

Viral components and nuclear transport proteins

Expression and purification of M1, M1¹⁻¹⁶⁵, M1¹⁶⁵⁻²⁵² and M1^{mutNLS} (Baudin *et al.*, 2001) and isolation of vRNP and NP from influenza virus A/PR/8/34 (Baudin *et al.*, 1994; Klumpp *et al.*, 1997) have been described. The DNA coding for NEP was PCR amplified from the gene encoding the alternative splice variant NS1 (influenza virus A/WSN/33) and subcloned into pET16b (Novagen) using sites *NdeI* and *XhoI*; deletion mutants NEP¹⁻⁵⁴, NEP⁵⁴⁻¹¹⁶ and NEP⁵⁴⁻¹²¹ were subcloned using a Mutagenesis Ex-site kit (Stratagene). NEP and mutant proteins were expressed as N-terminally His-tagged proteins in *E. coli* BL21(DE3) by induction with 0.5 mM isopropylthiogalactoside at 30°C for 4 h. Proteins were purified by Ni-NTA chromatography followed by gel filtration on Superdex 75 (Pharmacia) in 20 mM Tris-HCl pH 7.5 and 150 mM NaCl.

His-tagged Crm1 was expressed from a pQE60 plasmid in *E. coli* strain Tg1 by induction with 0.5 mM isopropyl-β-D-thiogalactopyranoside (IPTG) at 30°C for 4 h. His-tagged Snurportin 1 was expressed from a pQE30 plasmid in *E. coli* BL21(DE3) by induction with 0.1 mM IPTG for 4 h at 37°C. Both Crm1 and Snurportin 1 were purified on Ni-NTA-agarose, followed by monoQ chromatography and gel filtration on Superdex 200 (Pharmacia). Untagged Ran (Klebe *et al.*, 1995) and His-tagged Rna1p (Bischoff *et al.*, 1995) were purified as described.

Crystallization and structure determination

We obtained crystals of NEP⁵⁹⁻¹¹⁶ while attempting to crystallize a complex of NEP⁵⁹⁻¹¹⁶ bound to M1¹⁻¹⁶⁵. A complex of the two proteins purified by Superdex 75 chromatography (Pharmacia) was concentrated to 20 mg/ml. Despite the presence of M1¹⁻¹⁶⁵, crystals of the unbound NEP⁵⁹⁻¹¹⁶ species were obtained by hanging-drop vapour diffusion. The

high ionic strength of the precipitant (0.4 M ammonium di-phosphate) probably caused dissociation of the complex.

Heavy-atom derivatives were prepared by soaking crystals in 5 mM K₂PtCl₄ for 2 h (derivative I) or 4 h (derivative II), or in 5 mM K₂OsCl₆ (2 h) in 0.4 M ammonium diphosphate. Data were collected at 100K using 20% glycerol as the cryoprotectant on an ADSC area detector at ESRF beamline ID14-2. Data were processed using MOSFLM (Leslie *et al.*, 1992) and programs from the CCP4 suite (CCP4, 1994). Two heavy-atom sites were located in the platinum derivatives by SOLVE (Terwilliger and Berentzen, 1999), yielding an interpretable map after phase improvement with RESOLVE (Terwilliger, 2000) which automatically traced most of the main chain. Two low-occupancy Os sites were subsequently included for phasing at 2.8 Å resolution, and a final map was calculated to 2.6 Å resolution using non-crystallographic symmetry. Sixty-nine complete residues out of 116 were docked into the map by RESOLVE. The model was completed using O (Jones *et al.*, 1991) and refined using REFMAC (Winn *et al.*, 2001), treating the four helices of the dimer as independent TLS groups. The crystal packing was consistent with two possible choices of the biological dimer. However, the non-crystallographic dimer was easily assigned as the relevant one because of the large size and hydrophobic nature of its interface. Coordinates were deposited in the Protein Data Bank (accession No. 1PD3).

GTPase assays

Assays were performed as described (Bischoff *et al.*, 1995; Kutay *et al.*, 1997). First, 200 pmol of Ran were labelled with 30 nM [γ -³²P]GTP (5000 Ci/mmol). To measure substrate activities, 8 pmol of Ran [γ -³²P]GTP were incubated with 2 μM Crm1 and 0.001–20 μM of the tested substrate in a volume of 100 μl. After incubating for 15 min at 4°C, 10 μl aliquots of 0.1 μM Rna1p (the *Schizosaccharomyces pombe* RanGAP) were added to the mix and incubated for a further 2 min at 25°C. The reaction was stopped with 1 ml of activated charcoal and centrifuged (2 min at 12 000 g). Radioactivity in the supernatant was counted on a Wallac 1410 scintillation counter.

Pulldown assays

Twenty microlitres of magnetic Ni²⁺-agarose beads (Qiagen) preincubated (20 min, 20°C) with a His-tagged bait protein in 80 μl of buffer I (50 mM Tris-HCl pH 7.5, 5 mM imidazole, 300 mM NaCl, 15 mM MgCl₂), were incubated with an untagged prey protein in 160 μl of buffer I (30 min, 4°C). After washing twice with buffer I, beads were eluted with 20 μl of 20 mM Tris-HCl pH 7.5, 500 mM imidazole and 500 mM NaCl.

Acknowledgements

We thank Peter Askjaer and Iain Mattaj for providing clones for Crm1, Ran, Rna1p and snurportin1, Martine Moulin for help with protein purification and Steffi Arzt for help with data collection on ID14 (ESRF).

References

- Arzt,S., Baudin,F., Barge,A., Timmins,P., Burmeister,W.P. and Ruigrok,R.W.H. (2001) Combined results from solution studies on intact influenza virus M1 protein and from a new crystal form of its N-terminal domain show that M1 is an elongated monomer. *Virology*, **279**, 439–446.
- Askjaer,P., Heick Jensen,T., Nilsson,J., Engelmeier,L. and Kjems,J. (1998) The specificity of the CRM1-Rev nuclear export signal interaction is mediated by RanGTP. *J. Biol. Chem.*, **273**, 33414–33422.
- Baudin,F., Bach,C., Cusack,S. and Ruigrok,R.W.H. (1994) Structure of influenza RNP.I. Influenza virus nucleoprotein melts secondary structure in panhandle RNA and exposes the bases to solvent. *EMBO J.*, **13**, 3158–3165.
- Baudin,F., Petit,I., Weissenhorn,W. and Ruigrok,R.W.H. (2001) *In vitro* dissection of the membrane binding and RNP binding activities of influenza virus M1 protein. *Virology*, **281**, 102–108.
- Bischoff,F.R., Krebber,H., Smirnova,E., Dong,W. and Ponstingl,H. (1995) Co-activation of RanGTPase and inhibition of GTP dissociation by Ran-GTP binding protein RanBP1. *EMBO J.*, **14**, 705–715.
- Bui,M., Wills,E.G., Helenius,A. and Whittaker,G.R. (2000) Role of the influenza virus M1 protein in nuclear export of viral ribonucleoproteins. *J. Virol.*, **74**, 1781–1786.

- CCP4 (1994). The CCP4 suite: programs for protein crystallography. *Acta Crystallogr. D*, **50**, 760–763.
- Conti,E. and Kuriyan,J. (2000) Crystallographic analysis of the specific yet versatile recognition of distinct nuclear localization signals by karyopherin α . *Structure Fold Des.*, **8**, 329–338.
- Conti,E., Uy,M., Leighton,L., Blobel,G. and Kuriyan,J. (1998) Crystallographic analysis of the recognition of a nuclear localization signal by the nuclear import factor karyopherin α . *Cell*, **94**, 193–204.
- Elton,D., Simpson-Holley,M., Archer,K., Medcalf,L., Hallam,R., McCauley,J. and Digard,P. (2001) Interaction of the influenza virus nucleoprotein with the cellular CRM1-mediated nuclear export pathway. *J. Virol.*, **75**, 408–419.
- Fischer,U., Huber,J., Boelens,W.C., Mattaj,I.W., Luhrmann,R. (1995) The HIV-1 Rev activation domain is a nuclear export signal that accesses an export pathway used by specific cellular RNAs. *Cell*, **82**, 475–483.
- Fornerod,M., Ohno,M., Yoshida,M. and Mattaj,I.W. (1997) CRM1 is an export receptor for leucine-rich nuclear export signals. *Cell*, **90**, 1051–1060.
- Fukuda,M., Asano,S., Nakamura,T., Adachi,M., Yoshida,M., Yanagida,M. and Nishida,E. (1997) CRM1 is responsible for intracellular transport mediated by the nuclear export signal. *Nature*, **390**, 308–311.
- Huang,X.J., Hope,T.J., Bond,B.L., McDonald,D., Grahl,K. and Parslow,T.G. (1991) Minimal Rev-response element for type 1 human immunodeficiency virus. *J. Virol.*, **65**, 2131–2134.
- Jones,S. and Thornton,J.M. (1996) Principles of protein–protein interactions. *Proc. Natl Acad. Sci. USA*, **93**, 13–20.
- Jones,T.A., Zou,J.-Y., Cowan,S.W. and Kjeldgaard,M. (1991) Improved methods for building protein models in electron density maps and location of errors in these models. *Acta Crystallogr. A*, **47**, 110–119.
- Klebe,C., Prinz,H., Wittinghofer,A. and Goody,R.S. (1995) The kinetic mechanism of Ran–nucleotide exchange catalyzed by RCC1. *Biochemistry*, **34**, 12543–12552.
- Klumpp,K., Ruigrok,R.W.H. and Baudin,F. (1997) Roles of the influenza virus polymerase and nucleoprotein in forming a functional RNP structure. *EMBO J.*, **16**, 1248–1257.
- Kutay,U., Bischoff,F.R., Kostka,S., Kraft,R., Görlich,D. (1997) Export of importin α from the nucleus is mediated by a specific nuclear transport factor. *Cell*, **90**, 1061–1071.
- Lamb,R.A. and Krug,R.M. (2001) Orthomyxoviridae: the viruses and their replication. In Fields,B.N. *et al.* (eds), *Fields' Virology*, 4th edn. Lippincott–Raven, Philadelphia, PA, pp. 1487–1531.
- Leslie,A.G. (1992) Recent changes to the MOSFLM package for processing film and image plate data. In Wolf,W.M. and Wilson,K.S. (eds), *Joint CCP4 and ESF-EADBM Newsletter on Protein Crystallography*, No. 26. SERC Daresbury Laboratory, Warrington, UK.
- Liu,T. and Ye,Z. (2002) Restriction of viral replication by mutation of the influenza virus matrix protein. *J. Virol.*, **76**, 13055–13061.
- Lo Conte,L., Chothia,C. and Janin,J. (1999) The atomic structure of protein–protein recognition sites. *J. Mol. Biol.*, **285**, 2177–2198.
- Lommer,B.S. and Luo,M. (2002) Structural plasticity in influenza virus protein NS2 (NEP). *J. Biol. Chem.*, **277**, 7108–7117.
- Ma,K., Roy,A.M. and Whittaker,G.R. (2001) Nuclear export of influenza virus ribonucleoproteins: identification of an export intermediate at the nuclear periphery. *Virology*, **282**, 215–220.
- Malim,M.H. and Cullen,B.R. (1991) HIV-1 structural gene expression requires the binding of multiple Rev monomers to the viral RRE: implications for HIV-1 latency. *Cell*, **65**, 241–248.
- Malim,M.H., Bohnlein,S., Hauber,J., Cullen,B.R. (1989) Functional dissection of the HIV-1 Rev trans-activator—derivation of a trans-dominant repressor of Rev function. *Cell*, **58**, 205–214.
- Mann,D.A. *et al.* (1994) A molecular rheostat. Co-operative rev binding to stem I of the rev-response element modulates human immunodeficiency virus type-1 late gene expression. *J. Mol. Biol.*, **241**, 193–207.
- Martin,K. and Helenius,A. (1991) Nuclear transport of influenza virus ribonucleoproteins: the viral matrix protein (M1) promotes export and inhibits import. *Cell*, **67**, 117–130.
- Martin-Benito J., Area E., Ortega J., Llorca O., Valpuesta J.M., Carrascosa J.L. and Ortin J. (2001) Three-dimensional reconstruction of a recombinant influenza virus ribonucleoprotein particle. *EMBO Rep.*, **2**, 313–317.
- Meyer,B.E. and Malim,M.H. (1994) The HIV-1 Rev trans-activator shuttles between the nucleus and the cytoplasm. *Genes Dev.*, **8**, 1538–1547.
- Murti,K.G., Webster,R.G. and Jones,I.M. (1988) Localization of RNA polymerase on influenza viral ribonucleoproteins by immunogold labeling. *Virology*, **164**, 562–566.
- Neumann,G., Castrucci,M.R. and Kawaoka,Y. (1997) Nuclear import and export of influenza virus nucleoprotein. *J. Virol.*, **71**, 9690–9700.
- Neumann,G., Hughes,M.T. and Kawaoka,Y. (2000) Influenza A virus NS2 protein mediates vRNP nuclear export through NES-independent interaction with hCRM1. *EMBO J.*, **19**, 6751–6758.
- Nicholls,A., Sharp,K. and Honig,B. (1991) Protein folding and association: insight from the interfacial and thermodynamic properties of hydrocarbons. *Proteins*, **11**, 281–296.
- Ohno,M., Segref,A., Bachi,A., Wilm,M. and Mattaj,I.W. (2000) PHAX, a mediator of U snRNA nuclear export whose activity is regulated by phosphorylation. *Cell*, **101**, 187–198.
- O'Neill,R.E., Talon,J. and Palese,P. (1998) The influenza virus NEP (NS2 protein) mediates the nuclear export of viral ribonucleoproteins. *EMBO J.*, **17**, 288–296.
- Paragas,J., Talon,J., O'Neill,R.E., Anderson,D.K., Garcia-Sastre,A. and Palese,P. (2001) Influenza B and C virus NEP (NS2) proteins possess nuclear export activities. *J. Virol.*, **75**, 7375–7383.
- Paraskeva,E., Izzaualde,E., Bischoff,F.R., Huber,J., Kutay,U., Hartmann,E., Luhrmann,R. and Görlich,D. (1999) CRM1-mediated recycling of snurportin 1 to the cytoplasm. *J. Cell Biol.*, **145**, 255–264.
- Pleschka,S., Wolff,T., Ehrhardt,C., Hobom,G., Planz,O., Rapp,U.R. and Ludwig,S. (2001) Influenza virus propagation is impaired by inhibition of the Raf/MEK/ERK signalling cascade. *Nat. Cell Biol.*, **3**, 301–305.
- Ribbeck,K. and Görlich,D. (2002) The permeability barrier of nuclear pore complexes appears to operate via hydrophobic exclusion. *EMBO J.*, **21**, 2664–2671.
- Sha,B. and Luo,M. (1997) Structure of a bifunctional membrane-RNA binding protein, influenza virus matrix protein M1. *Nat. Struct. Biol.*, **4**, 239–244.
- Stade,K., Ford,C.S., Guthrie,C. and Weis,K. (1997) Exportin 1 (CRM1) is an essential nuclear export factor. *Cell*, **90**, 1041–1050.
- Terwilliger,T.C. (2000) Maximum likelihood density modification. *Acta Crystallogr. D*, **56**, 965–972.
- Terwilliger,T.C. and Berendzen,J. (1999). Automated MAD and MIR structure solution. *Acta Crystallogr. D*, **55**, 849–861.
- Thomas,S.L., Oft,M., Jaksche,H., Casari,G., Heger,P., Dobrovnik,M., Bevec,D. and Hauber,J. (1998) Functional analysis of the human immunodeficiency virus type 1 Rev protein oligomerization interface. *J. Virol.*, **72**, 2935–2944.
- Ward,A.C., Castelli,L.A., Lucantoni,A.C., White,J.F., Azad,A.A. and Macreadie,I.G. (1995) Expression and analysis of the NS2 protein of influenza A virus. *Arch. Virol.*, **140**, 2067–2073.
- Watanabe,K., Handa,H., Mizumoto,K. and Nagata,K. (1996) Mechanism for inhibition of influenza virus RNA polymerase activity by matrix protein. *J. Virol.*, **70**, 241–247.
- Watanabe,K., Takizawa,N., Katoh,M., Hoshida,K., Kobayashi,N. and Nagata,K. (2001) Inhibition of nuclear export of ribonucleoprotein complexes of influenza virus by leptomycin B. *Virus Res.*, **77**, 31–42.
- Weis,K. (2003) Regulating access to the genome: nucleocytoplasmic transport throughout the cell cycle. *Cell*, **112**, 441–451.
- Whittaker,G., Kemler,I. and Helenius,A. (1995) Hyperphosphorylation of mutant influenza virus matrix protein M1 causes its retention in the nucleus. *J. Virol.*, **69**, 439–445.
- Whittaker,G., Bui,M. and Helenius,A. (1996) Nuclear trafficking of influenza virus ribonucleoproteins in heterokaryons. *J. Virol.*, **70**, 2743–2756.
- Winn,M.D., Isupov,M.N. and Murshudov,G.N. (2001) Use of TLS parameters to model anisotropic displacements in macromolecular refinement. *Acta Crystallogr. D*, **57**, 122–133.
- Yasuda,J., Nakada,S., Kato,A., Toyoda,T. and Ishihama,A. (1993) Molecular assembly of influenza virus: association of the NEP protein with virion matrix. *Virology*, **196**, 249–255.
- Ye,Z., Robinson,D. and Wagner,R.R. (1995) Nucleus-targeting domain of the matrix protein (M1) of influenza virus. *J. Virol.*, **69**, 1964–1970.
- Ye,Z., Liu,T., Offringa,D.P., McInnis,J. and Levandowski,R.A. (1999) Association of influenza virus matrix protein with ribonucleoproteins. *J. Virol.*, **73**, 7467–7473.

Received April 25, 2003; revised July 9, 2003;
accepted July 23, 2003